Journal of Zhejiang University-SCIENCE A (Applied Physics & Engineering)
ISSN 1673-565X (Print); ISSN 1862-1775 (Online)
www.jzus.zju.edu.cn; www.springerlink.com
E-mail: jzus@zju.edu.cn

Simulation of the effects of non-Newtonian fluid on the behavior of a step hydraulic rod seal based on a power law fluid model*

Bing-qing WANG, Xu-dong PENG†‡, Xiang-kai MENG

College of Mechanical Engineering, Zhejiang University of Technology, Hangzhou 310032, China

†E-mail: xdpeng@zjut.edu.cn

Received Feb. 17, 2018; Revision accepted May 30, 2018; Crosschecked Oct. 10, 2018

Abstract: The rheological characteristics of the oil film on the rod-seal interface in the sealing zone have a major influence on the behavior of reciprocating seals. Because of the addition of polymers, the viscosity and temperature properties of hydraulic oil have improved and the fluid presents non-Newtonian characteristics. To investigate the influence of these characteristics on seal behavior, a soft elastohydrodynamic lubrication (EHL) numerical model is introduced to simulate a step seal under a mixed lubrication condition. A modified Reynolds equation is derived for calculating the fluid film pressure distribution more accurately. The equation is based on the power law fluid model and Jakobsson-Floberg-Olsson (JFO) cavitation theory. Results are presented to gain insight into the effect of non-Newtonian fluid characteristics on seal behavior, and the simulated results are compared to those of a Newtonian fluid to reveal the seal mechanism. The influence of operating parameters and the seal surface root mean square (RMS) roughness on sealing performance under different power law indexes is also investigated and discussed.

Key words: Non-Newtonian effect; Power law fluid; Step seal; Soft elastohydrodynamic lubrication (EHL)
https://doi.org/10.1631/jzus.A1800096 **CLC number:** TH117.2

1 Introduction

A reciprocating rod seal is a key element commonly used in hydraulic cylinders. Its function is to prevent hydraulic fluid leaking into the environment and to ensure the reliable performance of a hydraulic system. When the rod moves during both outstroke and instroke, the thin hydraulic oil film adhering to it is dragged into the sealing interface (i.e. the sealing zone) between the seal lip and the rod. The existing hydraulic oil in the sealing zone lubricates the seal and has a direct effect on the friction and leakage of the seal. A thick fluid film will lead to leakage, while a thin fluid film will result in a greater frictional force and exacerbate wearing of the seal. To gain a better understanding of the mechanism of action of such a seal and to realize accurate control of its working behavior, many researchers have carried out extensive theoretical and experimental studies since the 1960s (Nikas, 2010). As a result of their efforts, a lubrication theory of such seals has been successfully developed, covering full film lubrication (Stupkiewicz and Marciniszyn, 2009) and mixed lubrication (Salant et al., 2007; Öngün et al., 2008; Yang and Salant, 2010; Crudu et al., 2013; Li et al., 2018). The theory has been used to predict aspects of seal behavior, such as the film thickness (Karaszkiewicz, 1988; Field and Nau, 2008), pressure distributions (Ruskell, 1980; Green and English, 1994), and leakage and friction characteristics (Nikas, 2003; Heipl and Murrenhoff, 2015; Shen et al., 2015; Zhao et al., 2016).

‡ Corresponding author
* Project supported by the National Natural Science Foundation of China (Nos. 51575490 and 51775505), the National Basic Research Program (973 Program) of China (No. 2014CB046404), and the Zhejiang Provincial Natural Science Foundation of China (No. LZ15E050002)
ORCID: Bing-qing WANG, https://orcid.org/0000-0002-7004-9550; Xu-dong PENG, https://orcid.org/0000-0002-3502-7946
© Zhejiang University and Springer-Verlag GmbH Germany, part of Springer Nature 2018

All of those studies assumed the hydraulic oil was a Newtonian fluid. However, in practice, in an effort to improve the viscosity and temperature properties of lubricants, polymers are often added to the lubricating oils which make the oils exhibit a non-Newtonian fluid behavior (i.e., there is a non-linear relationship between the shear stress and the shear strain rate of the fluids) (Das, 1999). In addition, when the lubricant contains a small amount of gas (such as air bubbles), the rheological behavior of the lubricating oil will also deviate markedly from that of Newtonian fluids. Thus, the non-Newtonian rheological properties of lubricants have become an important factor in sealing design.

There have been many studies of the effect of non-Newtonian fluids on a number of critical tribological components, such as bearings (Dien and Elrod, 1983; Das, 1999; Sharma and Yadav, 2014), mechanical seals (Sinha et al., 1987; Safar, 1991), lip seals (Hajjam and Dominique, 2006), gears (Zhou et al., 2017), and magnetic heads/disks (Li et al., 1997). Various non-Newtonian fluid models have been proposed to predict the behavior of these lubricants, such as the power law model (Li et al., 1997; Sharma and Yadav, 2014), cubic law model (Kushare and Sharma, 2014), Herschel-Bulkley model (Bouyahia et al., 2006), couples stress model (Chippa and Sarangi, 2013), and micropolar model (Sharma and Rajput, 2013). The power law model (Eq. (1)), where the index n is related to the fluid flow behavior, is still the most commonly used in practice, since it can characterize two main types of non-Newtonian fluids, i.e. dilatant fluids ($n>1$) and pseudoplastic fluids ($0<n<1$). It can also characterize a Newtonian fluid ($n=1$), which is a hypothetical fluid widely used in numerical analysis (Das, 1999). In a previous study, Dien and Elrod (1983) derived a generalized steady-state Reynolds equation for 2D journal bearings using an equivalent power law model, which was the simplest power constitutive non-Newtonian fluid Reynolds equation of all. Li et al. (1997) proposed a modified average Reynolds equation to study the combined influence of the surface roughness and non-Newtonian fluids on the lubrication of a magnetic head-disk interface. In their study, the surface roughness was first taken into consideration by using the perturbation approach together with a Green's function. Other researchers such as Singh et al. (1982) have investigated the elastohydrostatic lubricating performance of a circular plate thrust bearing, under the condition of non-Newtonian power law fluids. They numerically analyzed the influence of the power law index n on the film profile and load capacity. Sharma and Yadav (2014) studied the effect of non-Newtonian fluids on the performance of a hybrid circular thrust pad bearing with various surface micro-dimples by introducing three key coefficients into a modified Reynolds equation, under several typical power law indexes (i.e. n=0.9, 1, 1.1).

In addition to the influence of non-Newtonian fluids on the behavior of hydraulic reciprocating rod seals, there are some other factors that cannot be ignored. Crudu et al. (2012), for example, used an inverse hydrodynamic lubrication theory to calculate the friction force of a U rod seal. Comparing their calculations with experimental data, they pointed out that the mixed lubrication condition should not be ignored for a very thin fluid film. In addition, according to the studies of Salant et al. (2007, 2010) on the simulation of a hydraulic reciprocating rod seal, the surface roughness of the seal lip plays an important role in determining the leakage and friction force of seals. They showed that a seal will encounter fluid cavitation near the air side at high rod speed during the outstroke. Thus, the mixed lubrication condition, as well as the effects of roughness and cavitation, should be taken into consideration in simulation research.

Based on the above points, in this study, we have derived a modified Reynolds equation based on the power law fluid model and Jakobsson-Floberg-Olsson (JFO) cavitation theory, which takes account of roughness, cavitation, and non-Newtonian fluid effects. To investigate the influence of the non-Newtonian flow characteristics of lubricating oil on the seal behavior of a hydraulic reciprocating step seal, a soft elastohydrodynamic lubrication (EHL) model coupled with fluid mechanics, contact mechanics, deformation analysis, and thermal analysis is used. Furthermore, the sealing mechanism of step hydraulic rod seals with two typical non-Newtonian fluids (i.e. a pseudoplastic fluid and a dilatant fluid) is compared to that of a Newtonian fluid, and the influence of some parameters (such as the rod speed, sealed pressure, and surface roughness of the seal) on sealing performance is also analyzed.

2 Theoretical models

2.1 Geometric model

A step hydraulic reciprocating rod seal was used to investigate the effect of non-Newtonian fluids with a soft EHL model. Fig. 1a shows the operating conditions of the rod seal in a linear hydraulic actuator. Under the action of the driving force caused by the hydraulic oil film pressure difference, the rod moves out of the cylinder during the outstroke and into the cylinder during the instroke. The oil side of the rod seal faces a low sealed pressure during the outstroke, and a high sealed pressure during the instroke. Generally, the sealed pressure on the oil side during the outstroke is relatively low and always equal to the ambient value, which was 0.1 MPa in this study.

Fig. 1b shows a schematic diagram of a step hydraulic reciprocating rod seal operating with a polished rod after the run-in period. The seal consists of a rubber elastomer O-ring, a polytetrafluoroethylene (PTFE)-based seal ring (i.e. the back-up ring), a sealing housing, and a rod. When a step seal is installed in a seal groove, the deformed O-ring pushes the PTFE-based seal ring to fit the rod closely, thus reducing or preventing the leakage of hydraulic oil.

Fig. 1c shows details of the sealing zone, which is the interface between the seal lip and the rod. It is reasonable to assume that the rod is perfectly smooth since the rod surface roughness is only one tenth of that of the seal lip surface, after the run-in polished period (Kanters and Visscher, 1989). In the sealing zone, a mixed lubrication condition occurs over the contact width L, which means that the seal achieves an equilibrium condition by the interaction of the asperity contact pressure p_c, fluid film pressure p_f, and static contact pressure p_{sc}. In addition, we assume that x represents the axial direction by neglecting the rod curvature, h is the nominal film thickness, and U is the constant rod speed, which has a positive value during the outstroke, but a negative value during the instroke. Generally, the contact angle of the seal lip on the hydraulic oil side is significantly larger than that on the air side (Fig. 4a). With this structure, the oil attached to the rod surface becomes easier to pump into the hydraulic cylinder again.

2.2 Soft EHL model

The numerical soft EHL model is schematically illustrated in the form of a block diagram (Fig. 2). All five components of the model, as well as the

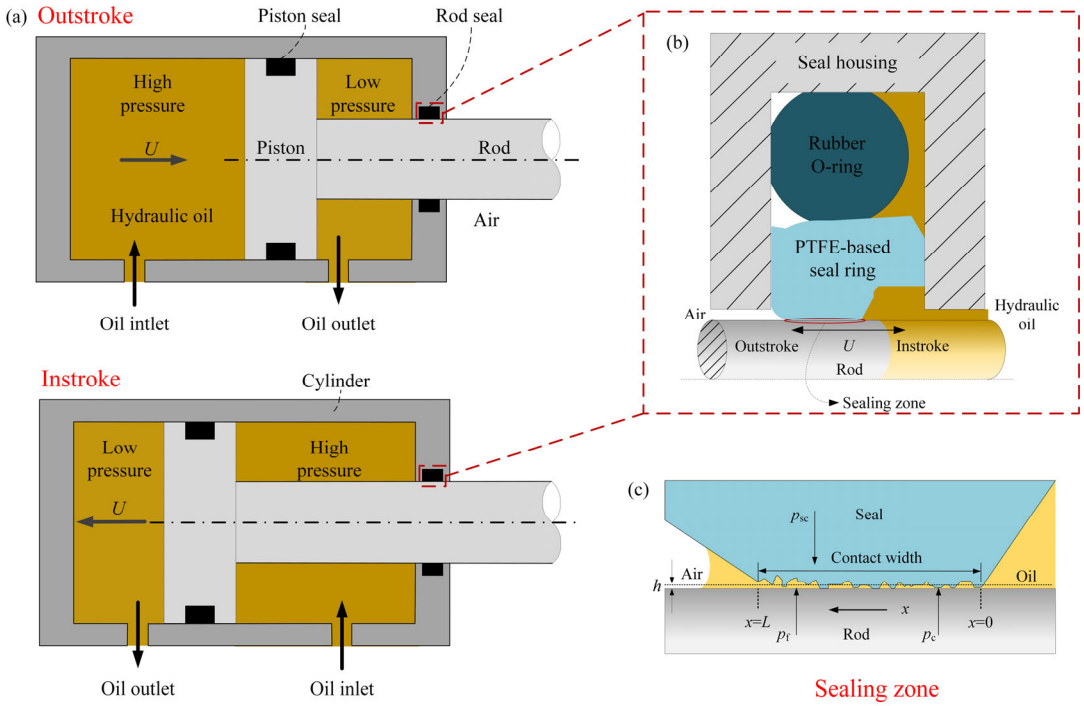

Fig. 1 Geometrical model

(a) Hydraulic seals in a linear hydraulic actuator; (b) Schematic of the step seal; (c) Details of the sealing zone

interactions between the components, are also presented. This model combines fluid mechanics with non-Newtonian fluids, static contact mechanics, asperity contact mechanics, deformation, and thermal analysis. The static contact mechanics are focused on calculating the length of the sealing zone (i.e. the contact width), static contact pressure, and the influence coefficient matrix by using an offline finite element analysis method in the commercial software ANSYS. A modified Reynolds equation based on the power law fluid model is used to yield the hydrodynamic fluid film pressure distribution in the sealing zone with the fluid mechanics analysis. The Greenwood-Williamson (G-W) model is applied to obtain the asperity contact pressure in a dynamic condition. In addition, the heat generated by the combination of the contact friction due to contact asperity and the viscous friction due to viscous shearing of the fluid, results in variation of the fluid viscosity in return.

We assumed that the effect of the micro-deformation of a step seal in the sealing zone resulting from the combination of the microscale fluid mechanics and microscale asperity contact mechanics on the macro-deformation of the seal is negligible, since the macro-deformation of the seal obtained by the static contact mechanics analysis is on a millimeter scale, while the micro-deformation of the seal is on a micrometer scale. Based on this assumption, the influence coefficient method is applied to update the film thickness in the micro-deformation analysis of the seal. The iteration continues until the film thickness converges, and then some other auxiliary results will be output, such as the leakage rate and friction force.

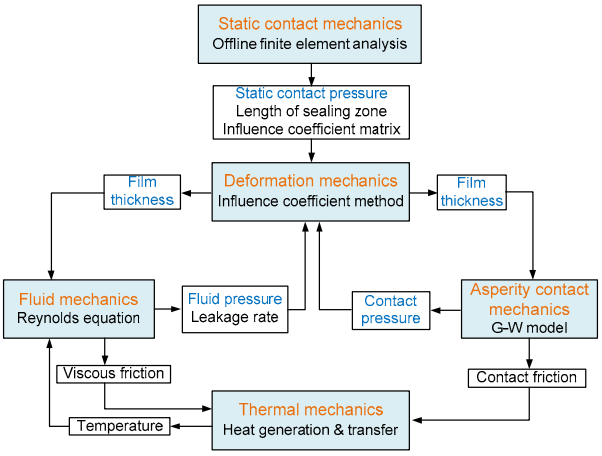

Fig. 2 Components of the numerical model

2.2.1 Fluid mechanics

Considering the flow of a power law fluid between two rough surfaces, z_1 and z_2, with translational velocities U_1 and U_2, respectively, in the x direction, the details of the frictional couple and the film are shown in Fig. 3a. The two rough surfaces are separated by the local film thickness $h_T=h+\delta_1+\delta_2$, where the nominal film thickness h represents the distance between the mean levels of two surfaces, and δ_1 and δ_2 are the random heights relative to the mean levels of two rough surfaces, respectively. In addition, z is the direction of the fluid film thickness (i.e. the normal direction of the x-y plane), and u, v, and w represent the velocities of the fluid in the x, y, and z directions, respectively.

$$\tau = m\left|\frac{\partial u}{\partial z}\right|^{n-1}\frac{\partial u}{\partial z} = \mu\frac{\partial u}{\partial z}, \tag{1}$$

where τ is the shear stress, m is the consistency coefficient, μ is the equivalent viscosity of the fluid, and n is the power law index. $0<n<1$, $n=1$, and $n>1$ characterize a pseudoplastic fluid (shear thinning), Newtonian fluid, and dilatant fluid (shear thickening), respectively.

Assuming the fluid is laminar, incompressible, and non-inertial, the momentum equations simplified from the Navier-Stokes equations take the form of

$$\frac{\partial}{\partial z}\left(\mu\frac{\partial u}{\partial z}\right) = \frac{\partial p}{\partial x}, \tag{2a}$$

$$\frac{\partial}{\partial z}\left(\mu\frac{\partial v}{\partial z}\right) = \frac{\partial p}{\partial y}, \tag{2b}$$

$$\frac{\partial p}{\partial z} = 0, \tag{2c}$$

where p is the fluid pressure.

The continuity equation of an incompressible fluid is given by

$$\frac{\partial u}{\partial x}+\frac{\partial v}{\partial y}+\frac{\partial w}{\partial z} = 0. \tag{3}$$

In the case of a rod-seal interface lubricated with a power law non-Newtonian fluid, $U_1=0$ and $U_2=U$. According to the perturbation procedure (Dien and Elrod, 1983), u and v can be obtained by

$$u=\frac{U}{h_{\mathrm{T}}}z-\frac{z\left(h_{\mathrm{T}}-z\right)}{2\mu_0}\frac{\partial p}{\partial x}\frac{1}{1+\dfrac{2I_0}{\mu_0}\left(\dfrac{\partial\mu}{\partial I}\right)_{I=I_0}}, \tag{4a}$$

$$v=-\frac{z\left(h_{\mathrm{T}}-z\right)}{2\mu_0}\frac{\partial p}{\partial y}, \tag{4b}$$

where I is the second invariant of the strain rate tensor, $I=(\partial u/\partial z)^2+(\partial v/\partial z)^2$, and $\mu=mI^{(n-1)/2}$. In addition, I_0 and μ_0 are the zero-order values, respectively, for the two variables mentioned above, in the expansion of the perturbation method.

By integrating the velocity of the fluid along the fluid film thickness, the flow rates (i.e. the volume flow per unit width) in the x and y directions can be respectively expressed by

$$q_x=\int_0^h u\mathrm{d}z=\frac{Uh_{\mathrm{T}}}{2}-\frac{h_{\mathrm{T}}^{n+2}}{12nmU^{n-1}}\frac{\partial p}{\partial x}, \tag{5a}$$

$$q_y=\int_0^h v\mathrm{d}z=-\frac{h_{\mathrm{T}}^{n+2}}{12mU^{n-1}}\frac{\partial p}{\partial y}. \tag{5b}$$

The mean flow rates entering the control volume (Fig. 3b) in the x and y directions, respectively, are given by Patir and Cheng (1978, 1979):

$$\overline{q}_x=\frac{1}{\Delta y}\int_y^{y+\Delta y}q_x\mathrm{d}y=-\phi_{xx}\frac{h^{n+2}}{12nmU^{n-1}}\frac{\partial\overline{p}}{\partial x}+\frac{U\overline{h}_{\mathrm{T}}}{2}+\frac{U}{2}\sigma\phi_{\mathrm{scx}}, \tag{6a}$$

$$\overline{q}_y=\frac{1}{\Delta x}\int_x^{x+\Delta x}q_y\mathrm{d}x=-\phi_{yy}\frac{h^{n+2}}{12mU^{n-1}}\frac{\partial\overline{p}}{\partial y}, \tag{6b}$$

where $\overline{h}_{\mathrm{T}}$ is the average truncated film thickness, $\overline{h}_{\mathrm{T}}=\int(h+\delta)f(\delta)\mathrm{d}\delta$, and $f(\delta)$ is the probability density function of $\delta=\delta_1+\delta_2$. ϕ_{xx}, ϕ_{yy}, and ϕ_{scx} are flow factors (Patir and Cheng, 1978, 1979). σ is the root mean square (RMS) roughness of the seal surface.

For a power law fluid, the conservation principle of the flow is given by

$$\frac{\partial\overline{q}_x}{\partial x}+\frac{\partial\overline{q}_y}{\partial y}=-\frac{\partial\overline{h}_{\mathrm{T}}}{\partial t}, \tag{7}$$

where t is the time.

By introducing Eqs. (6a) and (6b) into Eq. (7), the average flow Reynolds equation for a non-Newtonian power law fluid is as follows:

$$\frac{\partial}{\partial x}\left(\phi_{xx}\frac{h^{n+2}}{n}\frac{\partial\overline{p}}{\partial x}\right)+\frac{\partial}{\partial y}\left(\phi_{yy}h^{n+2}\frac{\partial\overline{p}}{\partial y}\right)=12mU^{n-1}\left[\frac{U}{2}\frac{\partial h_{\mathrm{T}}}{\partial x}+\sigma\frac{U}{2}\frac{\partial\phi_{\mathrm{scx}}}{\partial x}+\frac{\partial h_{\mathrm{T}}}{\partial t}\right]. \tag{8}$$

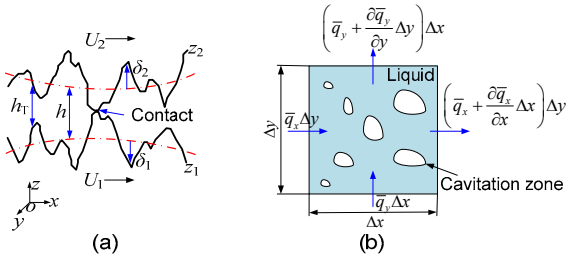

Fig. 3 Micro-scale fluid flow model
(a) Film geometry; (b) Control volume for average flow

In general, cavitation occurs when the local pressure of the fluid film is less than the local saturated vapor pressure (Fig. 3b). According to the literature, the JFO cavitation boundary condition can ensure mass conservation across the film rupture and reformation boundaries (Floberg, 1964), and is accurate in predicting the cavitation phenomenon of the fluid film (Payvar and Salant, 1992). Thus, in the present study, the JFO cavitation boundary condition was applied to Eq. (8), and the modified form of Eq. (8) (i.e. p-θ model) can be given as

$$\frac{\partial}{\partial x}\left(\phi_{xx}\frac{h^{n+2}}{n}\frac{\partial\overline{p}}{\partial x}\right)+\frac{\partial}{\partial y}\left(\phi_{yy}h^{n+2}\frac{\partial\overline{p}}{\partial y}\right)=6mU^n\frac{\partial\theta h_{\mathrm{T}}}{\partial x}+6GmU^n\sigma\frac{\partial\phi_{\mathrm{scx}}}{\partial x}+12mU^{n-1}\frac{\partial\theta h_{\mathrm{T}}}{\partial t}, \tag{9a}$$

with a complementary condition

$$\begin{cases}0<\theta<1,\ \overline{p}=p_{\mathrm{c}},\ G=0, & \text{in cavitation zone,}\\ \theta=1,\ \overline{p}>p_{\mathrm{c}},\ G=1, & \text{in liquid film zone,}\end{cases} \tag{9b}$$

where G is the cavitation index, and $\theta=\rho/\rho_{\mathrm{L}}$ is the density ratio. ρ is the density, and ρ_{L} is the fluid density.

To simplify the computational simulation, the 1D steady form of Eq. (9a) is used since the seal is axisymmetric and the film thickness is much smaller than the seal radius (Salant et al., 2007). Thus, the one-dimensionless form of Eq. (9a) is given by

$$\frac{\partial}{\partial X}\left(\phi_{xx}\frac{H^{n+2}}{n}\frac{\partial P}{\partial X}\right)=6\zeta\frac{\partial\theta H_{\mathrm{T}}}{\partial X}+6G\frac{\zeta\partial\phi_{\mathrm{scx}}}{\partial X}, \quad (10a)$$

with the complementary condition

$$\begin{cases}0<\theta<1,\ P=0,\ G=0, & \text{in cavitation zone,}\\ \theta=1,\ P>0,\ G=1, & \text{in liquid film zone,}\end{cases} \quad (10b)$$

where the dimensionless variables can be expressed as follows: $\zeta=mU^nL/(p_{\mathrm{a}}\sigma^{n+1})$, $P=(\overline{p}-p_{\mathrm{cav}})/(p_{\mathrm{a}}-p_{\mathrm{cav}})$, $X=x/L$, $H=h/\sigma$, and $H_{\mathrm{T}}=h_{\mathrm{T}}/\sigma$. p_{a} is the atmospheric pressure, and p_{cav} is the cavitation pressure.

Assuming that both the oil side and air side are fully flooded with fluids, then the following dimensionless boundary conditions are used to solve the fluid pressure, cavitation index, and density ratio:

$$\begin{cases}P=\dfrac{p_{\mathrm{s}}-p_{\mathrm{cav}}}{p_{\mathrm{a}}-p_{\mathrm{cav}}}=P_{\mathrm{s}},\ \theta=G=1, & X=0,\\ P=\dfrac{p_{\mathrm{a}}-p_{\mathrm{cav}}}{p_{\mathrm{a}}-p_{\mathrm{cav}}}=1,\ \theta=G=1, & X=1,\end{cases} \quad (11)$$

where p_{s} is the sealed pressure, and X=0 represents the oil side (Fig. 1c).

In addition, a more accurate Roelands equation is used to describe the viscosity-temperature-pressure relationship of the dynamic viscosity of the thin hydraulic oil (i.e. the consistency coefficient) (Roelands, 1966):

$$m=m_0\exp\left\{\left(\ln m_0+9.67\right)\times\left[-1+\left(1+5.1\times10^{-9}\overline{p}\right)^{z_0}\left(\frac{T-138}{T_0-138}\right)^{-s_0}\right]\right\}, \quad (12a)$$

$$z_0=\alpha\Big/\left[5.1\times10^{-9}\left(\ln m_0+9.67\right)\right], \quad (12b)$$

$$s_0=\beta\left(T_0-138\right)\Big/\left(\ln m_0+9.67\right), \quad (12c)$$

where m_0 is the consistency coefficient at atmospheric pressure and ambient temperature, and T_0 is the ambient temperature. α represents the pressure-viscosity coefficient, and β represents the viscosity-temperature coefficient.

In this study, assuming a Gaussian distribution for the seal lip surface asperity heights, the truncated film thickness can be calculated by

$$H_{\mathrm{T}}=\frac{H}{2}+\frac{H}{2}\mathrm{erf}\left(\frac{H}{\sqrt{2}}\right)+\frac{1}{\sqrt{2\pi}}\mathrm{e}^{\left(\frac{-H^2}{2}\right)}. \quad (13)$$

Eq. (10a) is a convection-diffusion-reaction equation. Therefore, an efficient and stable finite element method (FEM) algorithm, that is, a stream-upwind/Petrov-Galerkin (SUPG) weighted residual FEM, was applied to solve Eq. (10a) with Eq. (10b) (Meng et al., 2014a). According to the SUPG technology, the integral weak form of Eq. (10a) can be written as

$$\begin{aligned}&\int_{\Omega}\left[\phi_{xx}\frac{H^{n+2}}{n}\frac{\partial W}{\partial X}\frac{\partial P}{\partial X}\right]\mathrm{d}\Omega\\&-\int_{\Omega}\left[W\left(6\zeta\frac{\partial\left(\theta H_{\mathrm{T}}\right)}{\partial X}\right)\right]\mathrm{d}\Omega\\&+\int_{\Omega}\frac{1}{2}\tau^{\mathrm{SUPG}}\left(6\zeta\theta H_{\mathrm{T}}\right)^2\left(\frac{\partial W}{\partial X}\right)\left(\frac{\partial W}{\partial X}\right)\mathrm{d}\Omega\\&=-\int_{\Omega}6\zeta GW\frac{\partial\phi_{\mathrm{scx}}}{\partial X}\mathrm{d}\Omega,\end{aligned} \quad (14)$$

where W is the weight function, Ω is the computational domain, and SUPG is the stabilization parameter with the following expression (Zienkiewicz and Taylor, 2000):

$$\tau^{\mathrm{SUPG}}=\frac{h_{\mathrm{Triangle}}}{\left|6\zeta\right|}, \quad (15)$$

where h_{Triangle} is the characteristic length of each element in the direction of the velocity $\boldsymbol{U}(6\zeta, 0)$.

The detailed iterative procedure for solving Eq. (14) is given by Meng et al. (2014b), but there are some other differences. For example, the cavitation index should be involved in the iterative loop of the fluid pressure, and a more iterative loop is needed to achieve the viscosity convergence.

After the fluid pressure is obtained, the volumetric flow rate q of the step seal can be computed by

Eq. (16) and the average fluid viscous shear stress τ_f in the sealing zone by Eq. (17):

$$q=\frac{\pi D p_a \sigma^{n+2}}{12mU^{n-1}L}\left(-\phi_{xx}\frac{H^{n+2}}{n}\frac{\partial P}{\partial X}\right)+\frac{\pi D p_a \sigma^{n+2}\zeta}{2mU^{n-1}L}\left(\theta H_T+G\phi_{scx}\right), \tag{16}$$

$$\tau_f=\frac{mU}{h}\left(\phi_f-\phi_{fss}\right)-\phi_{fpp}\frac{h^n}{2U^{n-1}n}\frac{p_a}{L}\frac{\partial P}{\partial X}, \tag{17}$$

where D is the diameter of the rod. ϕ_f, ϕ_{fss}, ϕ_{fpp} are flow factors, which can be obtained from Patir and Cheng (1978, 1979).

2.2.2 Asperity contact mechanics

As mentioned above, the rod is deemed to be smooth because the rod surface is much smoother than that of the seal lip. According to the mixed lubrication theory, when the average fluid film thickness is less than 3σ, asperity contact will occur. Here, the statistical G-W approach is applied to predict the pressure due to the contacting asperities in a dynamic condition (Greenwood and Williamson, 1966). Assuming a Gaussian distribution for the heights of contacting asperities, the asperity contact pressure and the contact shear stress are given by

$$p_c=\frac{4}{3}\eta E' R^{1/2}\sigma^{3/2}\times\frac{1}{\sqrt{2\pi}}\int_{h/\sigma}^{\infty}\left(z-h/\sigma\right)^{3/2}e^{-z^2/2}dz, \tag{18}$$

$$\tau_c=-fp_c\left(\frac{U}{|U|}\right), \tag{19}$$

where η is the density of the seal surface asperity, R is the asperity radius, z is the height of the asperity, and f is the friction coefficient. E' represents the equivalent elastic modulus, which can be computed by

$$\frac{1}{E'}=\frac{1-\nu_1^2}{E_1}+\frac{1-\nu_2^2}{E_2}, \tag{20}$$

where E represents the elastic modulus and ν is Poisson's ratio, and subscripts 1 and 2 represent their values relating to the rod and seal, respectively.

2.2.3 Static contact mechanics

Trelleborg's step seal (RSKA00100) (Fig. 4a) was studied here. In this study, the material of the elastomer O-ring was polyurethane, which is a typical hyperelastic and nonlinear rubber material. Under the condition of a large strain, the stress of rubber will increase abruptly, showing a highly nonlinear characteristic. Thus, a two-parameter Mooney-Rivlin hyperelastic model was adopted to characterize the relation between the stress and strain for such material. The constitutive equation for the rubber material can be written as

$$\bar{W}=C_{10}\left(I_1-3\right)+C_{01}\left(I_2-3\right)+\frac{1}{d}\left(J-1\right)^2, \tag{21}$$

where $\bar{W}$ is the strain energy density, I_1 and I_2 are the first and the second deviatoric strain invariants, respectively, and J relates to the elastic deformation gradient. C_{10}, C_{01}, and d are the Mooney-Rivlin coefficients, which here are equal to 0.2 MPa, 6 MPa, and 0.000 279, respectively.

In addition, the material of both the sealing housing and the rod was 316L, with an elastic modulus of 210 GPa and a Poisson's ratio of 0.29. The material of the back-up ring was PTFE, with an elastic modulus of 200 MPa and a Poisson's ratio of 0.45. Considering that the elastic modulus of these materials is far greater than that of the rubber, the linear elastic model was used in the finite element analysis.

Fig. 4 shows the 2D axisymmetric finite element model of the step seal used in the commercial software ANSYS. The geometric shape of the step seal before deformation is shown in Fig. 4a. Under the interaction of the radial interference fit and hydraulic fluid pressure, the deformed seal is tightly attached to the rod surface (Fig. 4b). The contact width, where the seal meets the rod, is also called the sealing zone. The static contact pressures of the seal in the sealing zone under assembly state and compression state are shown in Fig. 4c, in which the static contact pressure is obtained without considering the fluid pressure within the interface of the sealed zone.

The solid higher-order 2D 8-node PLANE183 element is applied to the simulation of the seal deformation in ANSYS. An enhanced Lagrange contact algorithm is used to solve the static contact pressure. The mesh of the FEM model contains 11 065

elements, obtained by using a mesh refinement technique. Results illustrate that the deviation in static contact pressure is less than 0.6%, ranging from 11 065 to 105 280 elements.

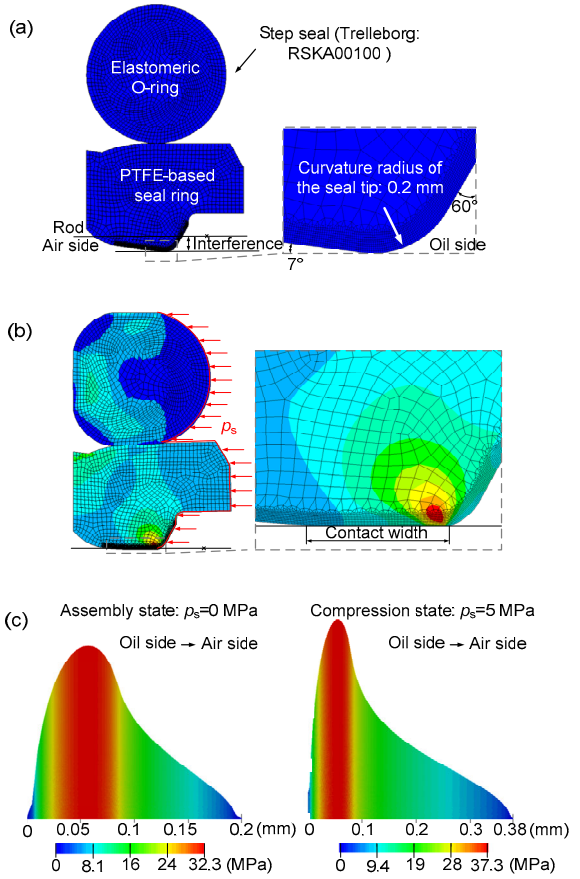

Fig. 4 FEM model of the step seal

(a) Seal before assembly; (b) Assembled lip on the rod (simulation results); (c) Static contact pressure

2.2.4 Micro-deformation mechanics

We assume that the mechanical behavior of the step seal is linear in the micro-deformation mechanics, since the variation of the film thickness is significantly smaller than the dimension of the seal itself, as discussed above. Thus, to improve computational efficiency, the influence coefficient method, which is based on small deformation theory, is applied to simulate the micro-deformation of the seal. With this method, the deformation of the seal at any location in the sealing zone is assumed proportional to the force applied at every location. The normal deformation of the lip surface can be calculated by

$$h_i = h_s + \sum_{k=1}^{n} (I_1)_{ik} \left(p_f + p_c - p_{sc} \right)_k , \tag{22}$$

where h_i represents the film thickness at the ith node, and p_f is the fluid pressure by solving Eq. (14). $(I_1)_{ik}$ represents the influence coefficient matrix, which is obtained by applying unit load to each node in the sealing zone (Fig. 5). h_s is the static film thickness, which is calculated by inverting Eq. (18) with p_{sc} and using a polynomial regression method (Streator, 2002).

2.2.5 Thermal analysis

During the movement of the rod, the heat generated by friction is produced mainly at the contacting surface (i.e. the sealing zone) due to the viscous shearing of the fluid and the asperity contact shear friction, and then conducted into the rod and seal. In this study, all the frictional heat is assumed to be transferred to the rod, since the thermal conductivity of the rod is much larger than that of the seal (Table 1). The effect of heat on the deformation of the seal is also not considered. Thus, the average steady-state temperature T_{ave} of the fluid film in the sealing zone can be computed using the following empirical formula (Bhushan, 1999):

$$T_{ave} - T_0 = \begin{cases} 1.07 \dfrac{(\tau_f + \tau_c) Ul}{k_{rod}} \left[\dfrac{\rho_r c_p Ul}{k_{rod}} \right]^{-1/2}, \\ \qquad\qquad \rho_r c_p Ul / k_{rod} > 0.68, \\ 0.64 \dfrac{(\tau_f + \tau_c) Ul}{k_{rod}} \ln \left[\dfrac{5.0 k_{rod}}{\rho_r c_p Ul} \right], \\ \qquad\qquad \rho_r c_p Ul / k_{rod} \le 0.68, \end{cases} \tag{23}$$

where l is the half length of the contact width, and k_{rod} is the thermal conductivity of the rod. ρ_r and c_p are the density and specific heat of the rod, respectively.

2.2.6 Auxiliary calculation

All the equations discussed above are strongly coupled (Fig. 2), so an interactive computational procedure is necessary. After the computations of the fluid film pressure and film thickness are converged, some of other auxiliary calculations, such as the fluid

transport per stroke (Q) and friction force on the rod (F), are performed:

$$Q=\int_0^{t_{\text{cycle}}} q\mathrm{d}t, \tag{24}$$

$$F=\pi D\int_0^L(\tau_{\text{f}}+\tau_{\text{c}})\mathrm{d}x. \tag{25}$$

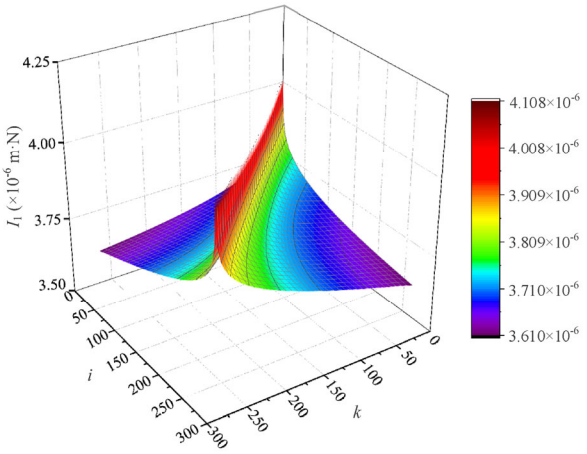

Fig. 5 Influence coefficient matrix

Table 1 Basic computational parameters

Parameter	Value
Diameter of the rod, D (mm)	10
Thermal conductivity of rod, k_{rod} (W/(m·K))	46
Specific heat of rod, c_{p} (J/(kg·K))	460
Density of rod, ρ_{r} (kg/m^3)	7900
Thermal conductivity of seal, k_{seal} (W/(m·K))	0.25
Sealed pressure, p_{s} (MPa)	0.1–20
Rod speed, U (m/s)	0.01–0.5
RMS roughness of seal, σ (μm)	0.4–1.6
Stroke length, L_{stroke} (mm)	100
Dry friction coefficient, f	0.1
Reference consistency coefficient, m_0 (Pa·s^n)	0.0608
Power law index, n	0.8–1.2
Pressure-viscosity coefficient, α (Pa^{-1})	2.10×10^{-8}
Viscosity-temperature coefficient, β (K^{-1})	3.18×10^{-2}
Ambient temperature, T_0 (K)	300

3 Results and discussion

In the following sections, the basic computational parameters listed in Table 1 are used for the step seal. The geometric and structural parameters of the step seal refer to the Trelleborg Company's products, and the properties of the hydraulic fluid and seal ring materials are given by Yang and Salant (2010). The parameters will remain unchanged in the subsequent analysis unless additional instructions are stated.

3.1 Seal behavior of non-Newtonian power law fluids

According to previous research, water was the first liquid medium used in the earliest hydraulic systems. Because of its poor lubricating properties, low viscosity, and corrosiveness, water was gradually replaced by mineral based hydraulic oil (Isaksson, 1987). Improvements made to the characteristics of hydraulic oil such as its anti-wear, low temperature, and high viscosity characteristics, mean that the amount and proportion of the anti-wear additives, corrosion inhibitors, and thickeners will be different. Therefore, the rheological behavior of hydraulic oil will also be changed correspondingly (i.e. the equivalent fluid viscosity, as well as the relationship between the shear stress and shear strain rate of fluids as shown in Eq. (1)). Thus, the effects of the consistency coefficient m_0 and power law index n on the seal behavior were the main object of this study.

Fig. 6 shows the contours of the sealing characteristics of a step seal under different values of both the consistency coefficient m_0 and power law index n, which are the most important parameters of the non-Newtonian power law fluid. The research scope of m_0 is 0.01–0.06 Pa·s^n, and n is 0.8–1.2 ($|U|$=0.3 m/s, σ=0.5 μm, and p_{s}=5.0 MPa). With increasing values of m_0, the volumetric flow rate q decreases gradually during the outstroke and instroke, while the friction force F increases slightly during the outstroke and decreases during the instroke. The effects of the power law index n on the volumetric flow rate q and friction force F are similar to that of the consistency coefficient m_0 (Fig. 6). For the larger values of n and m_0, the value of q during the instroke becomes negative and the absolute value of q is larger than that during the outstroke. This indicates that hydraulic oil is being pumped back to the cylinder again and the seal can meet zero leakage in this condition (Salant et al., 2007; Yang and Salant, 2010). When n is less than 1, the hydraulic oil is a pseudoplastic fluid, and it is difficult for the seal to achieve zero leakage under the conditions simulated.

In the analysis of the seal behavior of a non-Newtonian power law fluid, it can be seen that a hydraulic oil with a shear thickening rheological

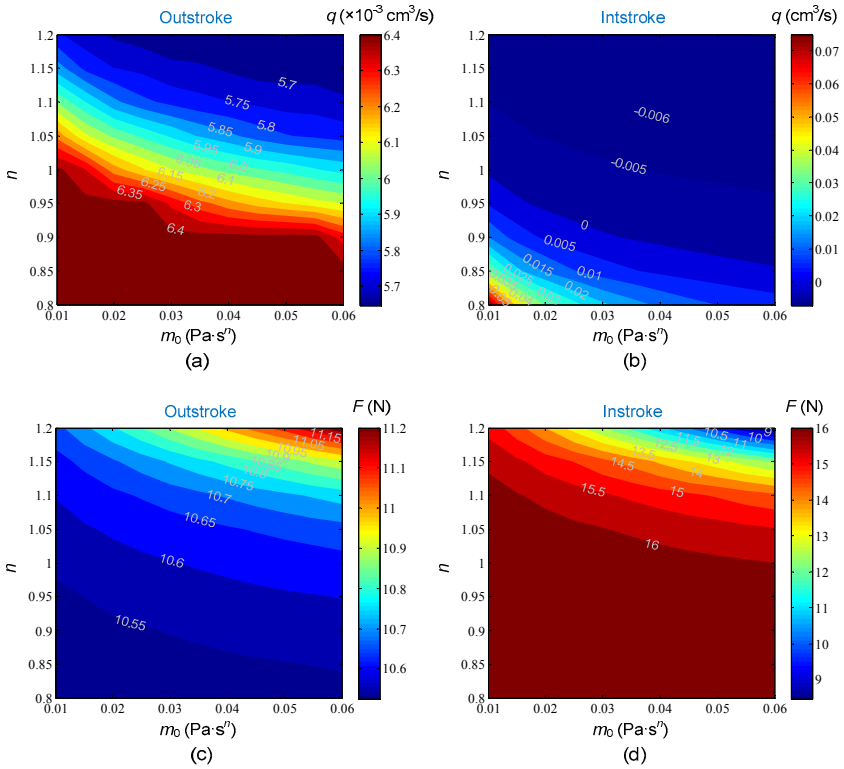

Fig. 6 Contours of sealing characteristics of a step seal in relation to the consistency coefficient m_0 and power law index n
(a) q, outstroke; (b) q, instroke; (c) F, outstroke; (d) F, instroke

property (i.e. a dilatant fluid) and a high consistency coefficient, is beneficial for the seal to prevent leakage. Comparing the degrees of influence of both the power law index and the consistency coefficient, it can be seen that the power law index seems to have a dominant influence on the seal behavior within the range of this research. In addition, as shown in Eq. (1), the power law index reflects the degree of the nonlinear relationship between the shear stress and shear strain rate of the fluid, while the consistency coefficient is more about the fluid viscosity (for example, when n=1.0, it represents the dynamic viscosity of the fluid). For a Newtonian fluid, it is generally acknowledged that the higher the fluid viscosity, the stronger is the hydrodynamic effect of a seal. What is more, there have already been many studies of the seal behavior of several hydraulic reciprocating seals with a Newtonian fluid assumption (Salant et al., 2007; Yang and Salant, 2010). Thus, to highlight the novelty of this study, the influences of three typical power law indexes, i.e. n=0.8 (pseudoplastic fluid), n=1.0 (Newtonian fluid), and n=1.2 (dilatant fluid), on the seal behavior will be described.

3.2 Sealing mechanisms of pseudoplastic fluid, Newtonian fluid, and dilatant fluid

From the above analysis, it can be seen that the rheological property of the hydraulic oil has a significant influence on the sealing performance of a step hydraulic reciprocating seal. Thus, to reveal this effect, detailed information about the sealing zone, such as the fluid pressure distribution and film thickness distribution, should be checked carefully.

Fig. 7 shows the fluid film pressure distribution in the sealing zone during both the outstroke and instroke with different power law indexes (i.e. n=0.8, 1.0, and 1.2). Here the RMS roughness of the seal surface σ is 0.5 μm, the sealed pressures p_s during the outstroke and instroke are 0.1 MPa and 5 MPa, respectively, and three different speeds of the rod, $|U|$=0.03, 0.1, and 0.3 m/s, are simulated. Note that the contact width of the sealing zone during the instroke is larger than that during the outstroke due to the increased sealed fluid pressure. When the power law index is n=1.2, the maximum value of the fluid pressure is much larger than when n=1.0 or n=0.8,

during both the outstroke and instroke. This means that the larger the value of the power law index, the stronger is the hydrodynamic effect of the seal.

During the outstroke, a peak is shown closer to the oil side of the seal in the fluid film pressure distribution, which is a significant characteristic of a

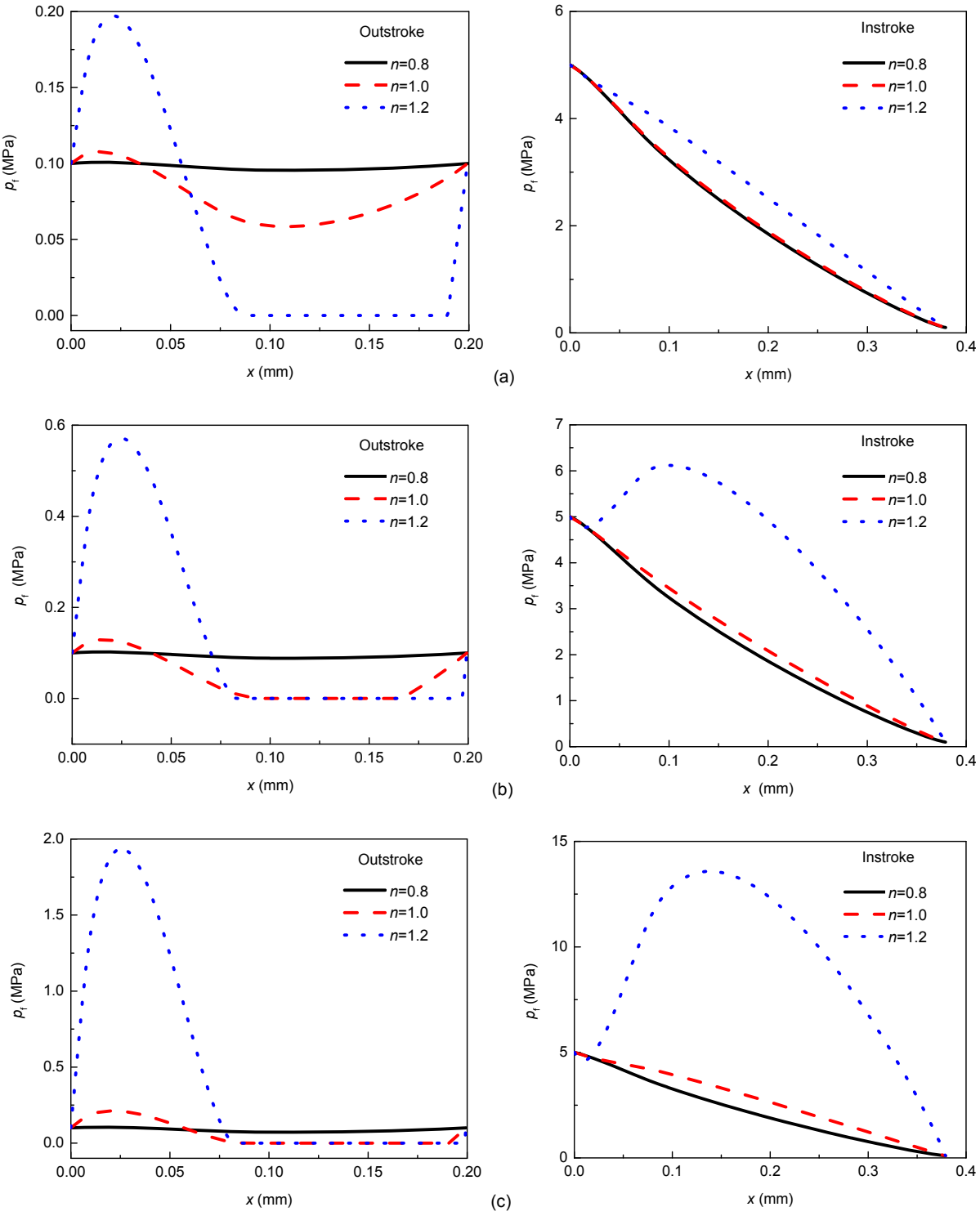

Fig. 7 Fluid pressure distribution with different power law indexes (σ=0.5 μm, p_s=5.0 MPa)
(a) $|U|$=0.03 m/s; (b) $|U|$=0.1 m/s; (c) $|U|$=0.3 m/s

successful hydraulic rod seal (Yang, 2010). In Fig. 7a, the rod speed is low and the pressure in the case of n=0.8 fluctuates near 0.1 MPa (atmospheric pressure) with a small amplitude, while there is a relatively large amplitude for n=1.0 or 1.2. Furthermore, the fluid film pressure goes to zero over-large portions of the sealing zone closer to the air side for n=1.2, indicating a cavitation. In Fig. 7b, when the rod speed is higher, the maximum value of the film pressure is greatly enhanced and the cavitation occurs in the case of n=1.0, indicating a strong hydrodynamic effect. In Fig. 7c, when the rod speed is the highest among the three cases, the hydrodynamic effect is further enhanced, and the cavitated fraction of the sealing zone for n=1.0 becomes the largest. Note that cavitation can restrict the flow of fluids through the sealing zone and inhibit the leakage of fluid, so that a better sealing performance of the seal can be achieved with more cavitation during the outstroke. During the instroke, the direction of the rod speed is opposite to that of the fluid pressure difference. For a low rod speed, i.e. $|U|$=0.03 m/s in Fig. 7a, the pressure profiles for n=0.8 and n=1.0 are concave, while it is convex for n=1.2. With $|U|$=0.1 m/s in Fig. 7b, the pressure firstly shows a valley then increases with a parabolic profile in the case of n=1.2, which can satisfy mass conservation. For a high rod speed, i.e. $|U|$=0.3 m/s in Fig. 7c, the maximum value of the fluid pressure for n=1.2 is more than double that shown in Fig. 7b, and the pressure profile for n=1.0 changes to convex. The above results show that the non-Newtonian power law fluid has a significant effect on the hydrodynamic effect; the dilatant fluid has a positive effect, while the pseudoplastic fluid has a negative effect compared to the Newtonian fluid.

The mechanism of the hydrodynamic effect with different power law indexes (i.e. n=0.8, 1.0, and 1.2) can be explained by examining the velocity profiles of the fluid film on the rod-seal interface. These are shown in Fig. 8 for n=0.8, 1.0, and 1.2 when the rod speed $|U|$=0.3 m/s during the instroke, since the fluid film pressure distributions differ greatly in this circumstance (Fig. 7c). Note that the bottom layer (h_T=0) and the upper layer of the fluid are on the rod and seal surfaces, respectively. In addition, the impact of the sealed pressure disturbance on the velocity distribution at the inlet and outlet of the sealing zone is not considered here. From Fig. 8 we can see that the trends of the velocity distributions are similar at different power law indexes n. At any location in the x-axis, the velocity of the fluid film decreases from 0.3 m/s to 0 m/s as the value of h_T increases. The pressure gradient along the direction through the film thickness has not been taken into consideration, so the velocity of the fluid varies with the average truncated film thickness h_T in a linear fashion, which can be judged from Eq. (4a). From Figs. 8a–8c, it is difficult to make an intuitive judgment as to which of these power law indexes (i.e. n=0.8, 1.0, and 1.2) has a larger fluid velocity distribution because its film thickness in the sealing zone is also different. The fluid velocity profiles in the sealing zone at h_T= 0.4 μm are shown in Fig. 8d. Clearly, the case of n=1.2 has the largest fluid film velocity distribution among the three cases, and n=0.8 has the smallest, indicating a higher viscous shearing of the fluid with increasing n since the rod surface speed always equals 0.3 m/s, which can also be determined by Eq. (1). In addition, the film thickness for n=1.2 is also larger than that of the other two cases. Thus, there is no doubt that the hydrodynamic effect due to the viscous shearing of the fluid for n=1.2 is the strongest, while the case of n=0.8 is the weakest among the analyses, which is consistent with that shown in Fig. 7. We conclude that variation in the power law index of non-Newtonian fluids or the fluid rheological property alters the flow behavior of the lubricant, especially the fluid film velocity profile, which is responsible for generating the fluid hydrodynamic pressure.

Figs. 9a and 9b present the film thickness and contact pressure distributions in the sealing zone during both the outstroke and instroke, respectively, for n=0.8, 1.0, and 1.2 at $|U|$=0.3 m/s. These figures show more detailed information on the rod-seal interface, which is in agreement with the results shown in Fig. 7c. Clearly, the greatest proportions of the sealing zone for the seal during both the outstroke and instroke are in a mixed lubrication, since the ratio of film thickness to RMS surface roughness is less than 3. During the outstroke, the film thickness distribution has a parabolic shape and is asymmetric about the x-axis, and the curve of the contact pressure distribution shows a bell-shaped profile. At x=0.057 mm, the film thickness begins to increase and the contact pressure reaches its maximum value. During the instroke, the trends of the film thickness and contact

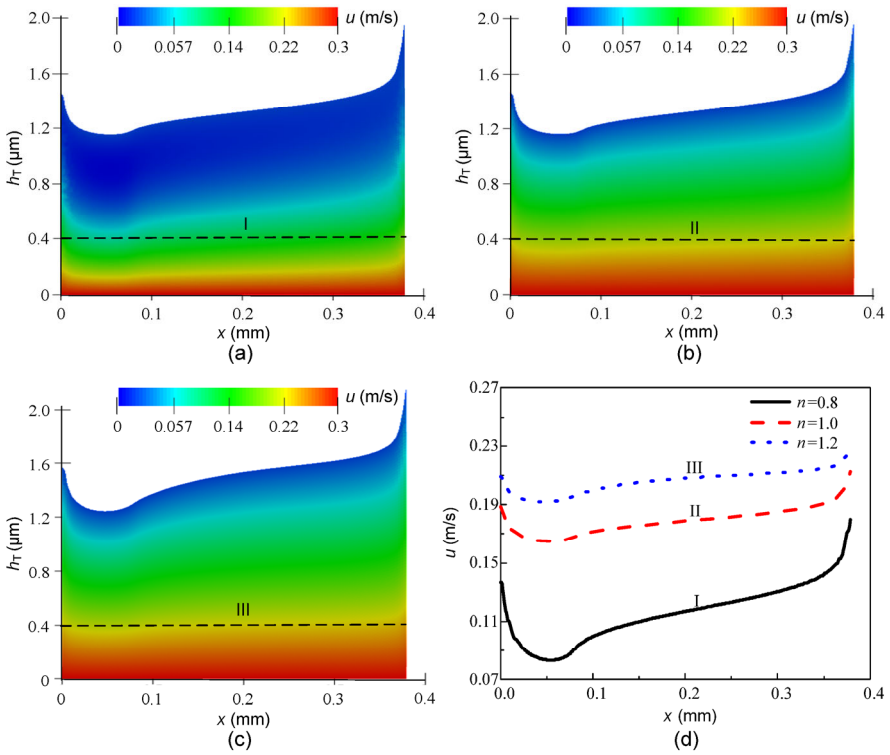

Fig. 8 Fluid film velocity distribution with different power law indexes (instroke, $|U|$=0.3 m/s, σ=0.5 μm, and p_s=5.0 MPa)
(a) n=0.8; (b) n=1.0; (c) n=1.2; (d) Fluid velocity profiles at h_T=0.4 μm

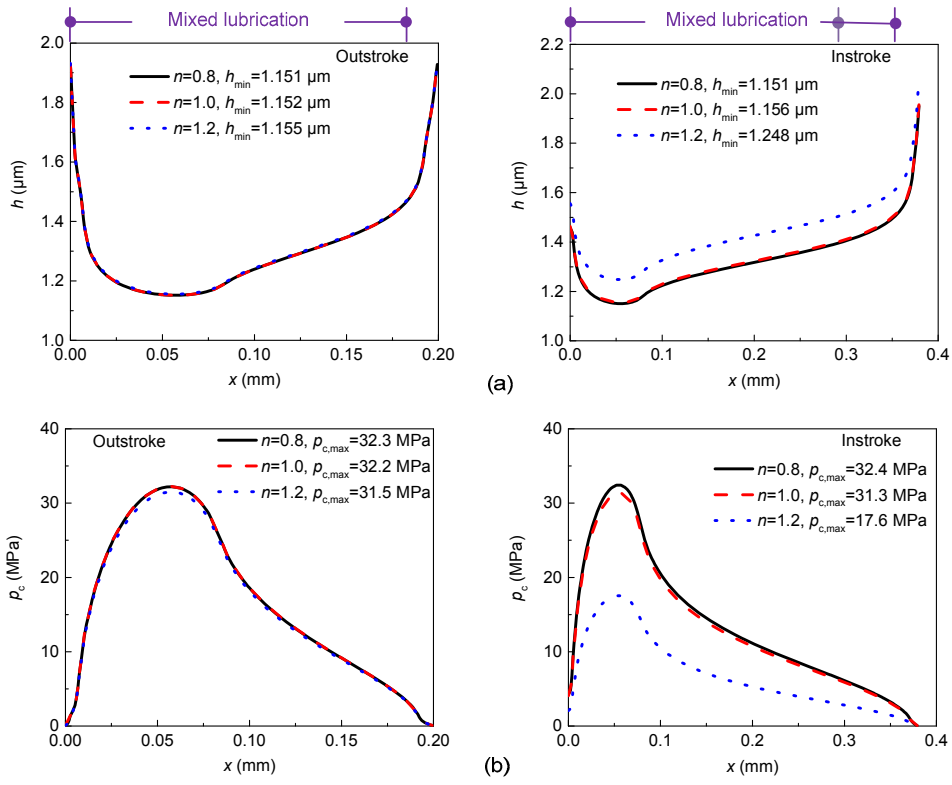

Fig. 9 Film thickness (a) and contact pressure (b) distributions with different power law indexes ($|U|$=0.3 m/s, σ=0.5 μm, and p_s=5.0 MPa)

pressure distributions are similar to those during the outstroke. However, the mixed lubrication region is larger than that during the outstroke, indicating a relatively poor lubricating condition. At x=0.057 mm, the film thickness decreases to its minimum value and the contact pressure becomes maximum. In addition, when the value of the power law index becomes larger, the film thickness increases and the contact pressure decreases. During the outstroke, the film thickness and contact pressure distributions of the seal are almost identical due to a very small fluid pressure difference. During the instroke, the film thickness in the case of n=1.2 is obviously larger than that in the case of n=0.8 or 1.0, and there is a correspondingly lower contact pressure.

The above results illustrate that the hydrodynamic effect due to the viscous shearing of the fluid is enhanced for a dilatant fluid, but is weakened for a pseudoplastic fluid, compared to a Newtonian fluid under the same conditions. They also mean that a dilatant fluid or a relatively large flow index is recommended for the application of a hydraulic reciprocating seal, and the use of a pseudoplastic fluid should be avoided since the excessive poor lubricating condition will result in a high risk of failure due to wear.

3.3 Effects of U, p_s, and σ on sealing performance

Fig. 10 shows the effect of the rod speed U on sealing performance. From Fig. 10a we can see that the volumetric flow rate q is above 0 and linearly increases with increasing U for different n during the outstroke, indicating a leaked condition. Note that the hydrodynamic effect becomes stronger with increasing U because a greater viscous shearing stress of the fluid is generated in the lubricant. As a result, more fluid tends to flow into the gap between the rod surface and the seal lip surface, leading to an increased leakage rate. The leakage rates during the outstroke are very similar for n=0.8, 0.9, 1.0, and 1.2 when U<0.2 m/s. When the power law index increases, the hydrodynamic effect due to the viscous shearing of the fluid increases, as discussed in Section 3.2. This results in decreased leakage because cavitation is occurring, restricting the flow. During the instroke, q almost decreases with increasing U for different values of n due to the enhanced hydrodynamic effect. For the case when n=0.9, 1.0 or 1.2, q is negative with increasing U, indicating that the leaked fluid is pumped back into the cylinder. It is generally considered that the characteristics of the fluid film forming during the outstroke are different from those during the instroke. Limiting the outflow of the fluid and drawing back the fluid adhering to the rod surface are two key features of a successful reciprocating seal (Nikas, 2010). A zero leakage rate is normally considered to have been achieved when the flow rate (must be negative value) of the seal during the instroke is not less than that during the outstroke. Under the conditions simulated, the minimum rod speed with zero leakage rate is about 0.388 m/s for n=1.0, and 0.041 m/s for n=1.2 (Fig. 10a).

Fig. 10b shows the friction force on the rod surface with different values of U for n=0.8, 0.9, 1.0, and 1.2, during both the outstroke and instroke. Under the mixed lubrication condition, the generation of frictional force is governed by the combined effect of the viscous shearing and the asperity contact. With increasing U, the friction force increases linearly during the outstroke and decreases during the instroke. This is caused mainly by increasing viscous shearing stress and decreasing asperity contact friction, respectively. The friction force is much larger during the instroke than during the outstroke, except in the case n=1.2 with U>0.26 m/s under the conditions simulated. This is because, on the one hand, the contact width during the instroke is larger than that during the outstroke due to the increased sealed fluid pressure, which indicates much greater generation of asperity contact friction. On the other hand, for the case of n=1.2, the oil is a dilatant fluid and has a shear thickening property. The oil film in the sealing zone forms more easily under a larger pressure difference and a higher rod speed (Fig. 9a), thus creating a smaller friction force. These findings for the case n=1.0 (i.e. the Newtonian fluid) are in accordance with previous studies (Yang, 2010; Yang and Salant, 2010).

Fig. 11 shows the influence of the sealed pressure p_s on sealing performance with different n. The net fluid transport per cycle Q, as defined in Eq. (24) and used to characterize the seal property with a steady simulation (Yang and Salant, 2010), and the average friction force F_{ave} (i.e. the average value of friction force during both the outstroke and instroke)

increase with increasing p_s. Yang and Salant (2010) proposed the above phenomenon for a Newtonian fluid (i.e. n=1.0) and gave a clearly explanation of why this happens. But for a non-Newtonian fluid, there are some significant differences in sealing performance due to the different rheological properties (Fig. 11). When n=0.8 or n=0.9, the oil is a pseudo-plastic fluid and the fluid transport (leakage) is much greater than when n=1.0, due to the weaker hydrodynamic effect. When n=1.2, the oil is a dilatant fluid with a shear thickening property, and the value of the net fluid transport falls below 0 with increasing U because more fluid is pumped back, and the seal achieves zero leakage (Fig. 11a). In addition, the net fluid transport of the seal for $|U|$=0.03 m/s is greater than that for $|U|$=0.1 m/s. This is reasonable because the leaking time is long under a low rod speed condition with a constant stroke length, and has a dominant influence compared to the hydrodynamic effect caused by viscous shearing of the fluid. The average friction force on the rod surface when n=0.8 or n=0.9 is very similar to that when n=1.0 and seems to be independent of U under the conditions simulated. This characteristic can be explained by Fig. 10b, since the friction force varies little with the rod speed during both the outstroke and instroke. For the case n=1.2, the increasing trend of the average friction force with increasing p_s is very different from the other two cases, since the hydrodynamic effect is strong and available at low rod speeds.

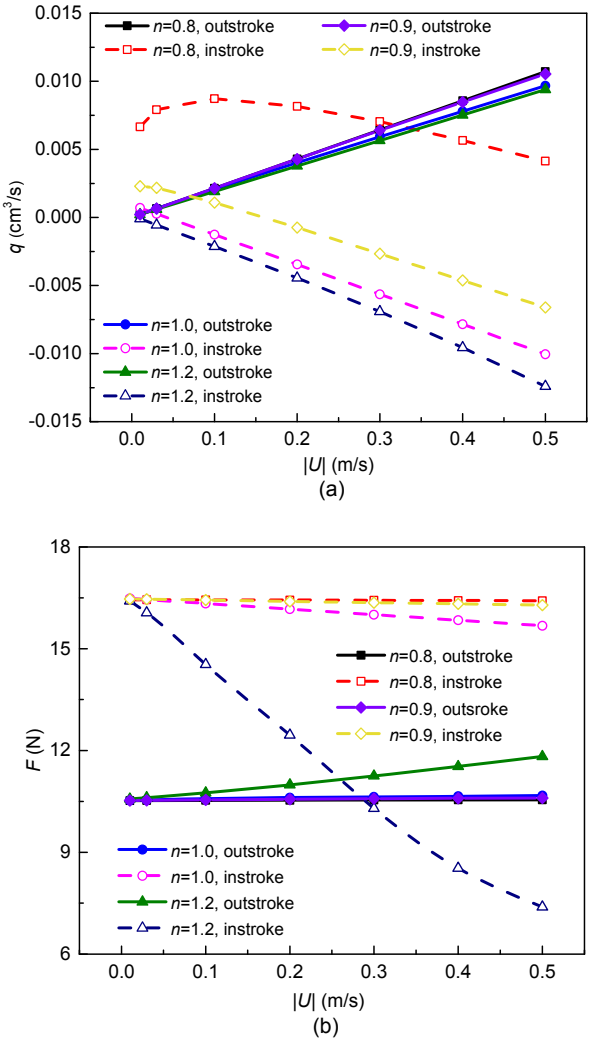

Fig. 10 Effect of U on sealing performance (σ=0.5 μm and p_s=5.0 MPa): (a) leakage rate; (b) friction force

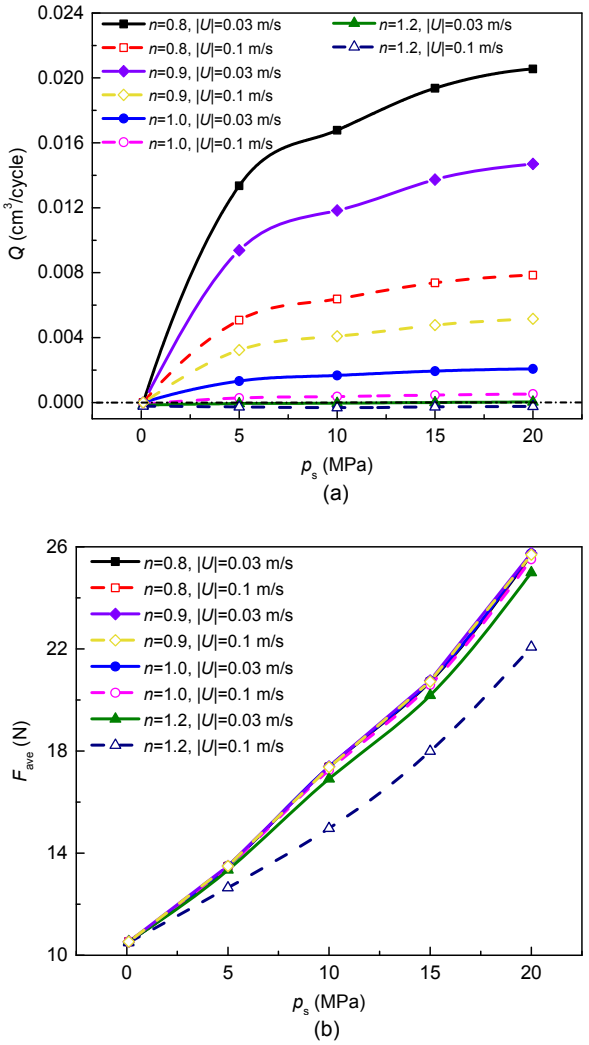

Fig. 11 Effect of p_s on sealing performance (σ=0.5 μm)
(a) Net fluid transport per cycle; (b) Average friction force

Fig. 12 presents the influence of the RMS roughness of the seal lip surface σ on sealing performance with different n. According to Salant et al. (2010), both the net fluid transport per cycle and the average friction force increase with increasing roughness, which is identical to the observed trend and provides a validation of the results shown in Fig. 12 for the case n=1.0 (i.e. the Newtonian fluid). In the case n=0.8 or n=0.9, the net fluid transport increases exponentially with increasing roughness, and the average friction force shows a slightly increasing trend. In this circumstance, the seal is generally in the leaking state. In the case n=1.2, the average friction force increases sharply when σ<0.7 μm and then increases gently with increasing RMS roughness σ of the seal surface. In addition, the value of the net fluid transport varies relatively little with increasing σ compared to a Newtonian fluid, and the seal appears to be in a state of zero leakage. This is also a consequence of the hydrodynamic effect due to the viscous shearing of the fluid. According to the results shown in Fig. 12b, we also find that among the four cases of n=0.8, 0.9, 1.0, and 1.2, the average friction force for n=1.2 is minimum when σ<1.0 μm, and becomes maximum when σ>1.2 μm. This is because, when the RMS surface roughness σ is small, the fluid for n=1.2 shows a shear thickening property, the hydrodynamic effect is strong, and thus the asperity contact friction is greatly reduced. When the RMS surface roughness σ is high, the asperity contact friction dominates and the total friction force increases slightly with increasing n with the effect of the viscous shearing of the fluid. In addition, the effect of the surface roughness on the sealing performance with different n for p_s=5 MPa is very similar to that of p_s=15 MPa, which agrees with the laws shown in Fig. 11.

The above parametric analysis reveals that, for a pseudoplastic lubricant with a shear thinning property, the hydrodynamic effect is relatively weak compared to that of a Newtonian fluid, and leads to leakage and a high friction force, especially under conditions of low rod speed, high sealed pressure, and large RMS surface roughness of the seal. For a dilatant lubricant with a shear thickening property, the hydrodynamic effect is greatly enhanced. It seems that the seal becomes sensitive to the operating parameters and presents a low leakage or even zero leakage state under a high rod speed and a small RMS roughness condition. The friction characteristics of the seal can also be improved because more fluid tends to share the load when n>1.

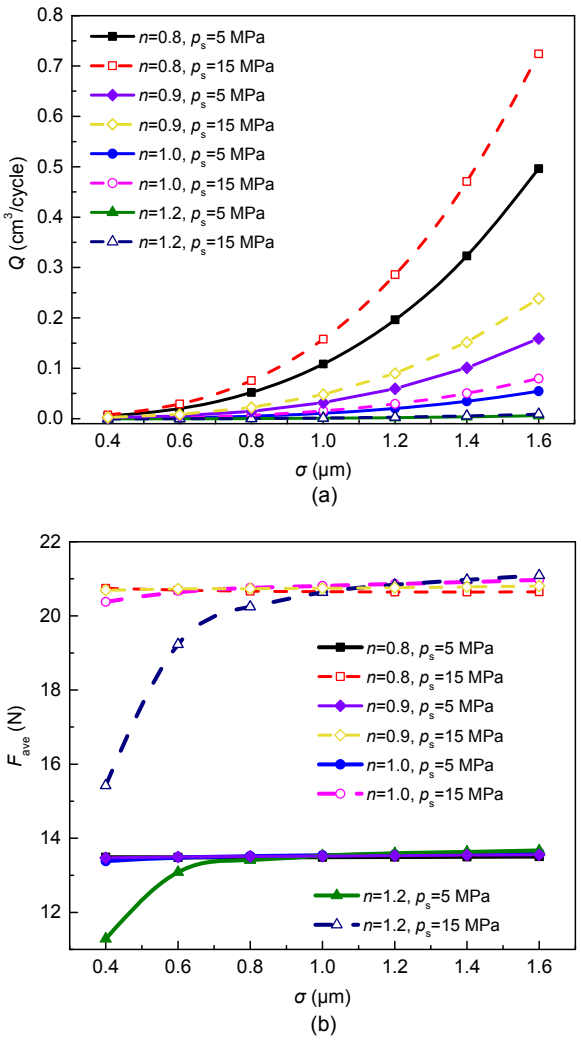

Fig. 12 Effect of σ on sealing performance ($|U|$=0.1 m/s)
(a) Net fluid transport per cycle; (b) Average friction force

4 Conclusions

In this study, a mathematical model was developed for a hydraulic reciprocating rod seal to analyze the effect of non-Newtonian fluids on the seal behavior. A modified Reynolds equation that takes the effects of roughness, fluid cavitation, and non-Newtonian fluid properties into consideration was derived based on the power law fluid model and JFO

cavitation theory, and was solved using the SUPG weighted residual finite element method. A mixed-lubrication soft EHL numerical model that considers coupled fluid mechanics, asperity contact mechanics, static contact mechanics, micro-deformation mechanics, and thermal analysis was presented to simulate the seal behavior of a step seal under steady conditions. This study concentrated primarily on the effect of non-Newtonian fluid properties, especially the power law index, on the seal behavior. The influences of the rod speed and the sealed pressure, as well as the RMS surface roughness of the seal under four fluid lubrication conditions (i.e. n=0.8, 0.9, 1.0, and 1.2) were also investigated.

Results showed that the non-Newtonian fluid effect has a significant influence on the film forming between the sealing interfaces, and on the sealing performance. The rheological properties of the hydraulic oil influence the viscous shearing stress of the fluid, resulting in a change in the hydrodynamic pressure. The hydrodynamic effect due to the viscous shearing of the fluid increases with the power law index. For a dilatant fluid, the hydrodynamic effect is strong due to the shear thickening rheological property, resulting in a seal with low friction and zero leakage. But for a pseudoplastic fluid, the lubrication condition in the sealing zone is relatively poor, and it is very difficult for the seal to achieve zero leakage under the conditions simulated. According to the analysis of the influence of the operating parameters on sealing performance, the non-Newtonian fluid effect of hydraulic oil on a reciprocating seal is not negligible, since the predicted values for both the leakage and friction force for the case n=0.8, 0.9 or 1.2 are substantially different from that of the case n=1.0 (i.e. a Newtonian fluid commonly used in calculations).

References

Bhushan B, 1999. Principles and Applications of Tribology. Wiley, New York, USA, p.403-444.

Bouyahia F, Hajjam M, Khlifi ME, et al., 2006. Three-dimensional non-Newtonian lubricants flows in sector-shaped, tilting-pads thrust bearings. *Proceedings of the Institution of Mechanical Engineers, Part J: Journal of Engineering Tribology*, 220(4):375-384. https://doi.org/10.1243/13506501JET92

Chippa SP, Sarangi M, 2013. Elastohydrodynamically lubricated finite line contact with couple stress fluids. *Tribology International*, 67:11-20. https://doi.org/10.1016/j.triboint.2013.06.014

Crudu M, Fatu A, Cananau S, et al., 2012. A numerical and experimental friction analysis of reciprocating hydraulic 'U' rod seals. *Proceedings of the Institution of Mechanical Engineers, Part J: Journal of Engineering Tribology*, 226(9):785-794. https://doi.org/10.1177/1350650112445973

Crudu M, Fatu A, Hajjam M, et al., 2013. Numerical and experimental study of reciprocating rod seals including surface roughness effects. *Sealing Technology*, 2013(6): 8-11. https://doi.org/10.1016/S1350-4789(13)70224-1

Das NC, 1999. A study of optimum load capacity of slider bearings lubricated with power law fluids. *Tribology International*, 32(8):435-441. https://doi.org/10.1016/S0301-679X(99)00072-9

Dien IK, Elrod HG, 1983. A generalized steady-state Reynolds equation for non-Newtonian fluids, with application to journal bearings. *ASME Journal of Tribology*, 105(3): 385-390. https://doi.org/10.1115/1.3254619

Field GJ, Nau BS, 2008. A theoretical study of the elastohydrodynamic lubrication of reciprocating rubber seals. *Tribology Transactions*, 18(1):48-54. https://doi.org/10.1080/05698197508982746

Floberg L, 1964. Cavitation in lubricating oil films. *In*: Davies R (Ed.), Cavitation in Real Liquids. Elsevier, New York, USA, p.138-146.

Green I, English C, 1994. Stresses and deformation of compressed elastomeric O-ring seals. 14th International Conference on Fluid Sealing, p.83-95.

Greenwood JA, Williamson JBP, 1966. Contact of nominally flat surfaces. *Proceedings of the Royal Society A: Mathematical, Physical & Engineering Sciences*, 295(1442):300-319. https://doi.org/10.1098/rspa.1966.0242

Hajjam M, Dominique B, 2006. Non-Newtonian effects on elastohydrodynamic behaviour of rotary lip seals. *Proceedings of the Institution of Mechanical Engineers, Part J: Journal of Engineering Tribology*, 220(2):79-85. https://doi.org/10.1243/13506501JET91

Heipl O, Murrenhoff H, 2015. Friction of hydraulic rod seals at high velocities. *Tribology International*, 85:66-73. https://doi.org/10.1016/j.triboint.2015.01.002

Isaksson O, 1987. Rheology for water-based hydraulic fluids. *Wear*, 115(1-2):3-17. https://doi.org/10.1016/0043-1648(87)90193-1

Kanters AFC, Visscher M, 1989. Lubrication of reciprocating seals: experiments on the influence of surface roughness on friction and leakage. *Tribology*, 14:69-77. https://doi.org/10.1016/S0167-8922(08)70182-2

Karaszkiewicz A, 1988. Hydrodynamic lubrication of rubber seals for reciprocating motion; leakage of seals with an O-ring. *Tribology International*, 21(6):361-367. https://doi.org/10.1016/0301-679X(88)90113-2

Kushare PB, Sharma SC, 2014. Nonlinear transient stability

study of two lobe symmetric hole entry worn hybrid journal bearing operating with non-Newtonian lubricant. *Tribology International*, 69:84-101. https://doi.org/10.1016/j.triboint.2013.08.014

Li WL, Weng CI, Hwang CC, 1997. An average Reynolds equation for non-Newtonian fluid with application to the lubrication of the magnetic head-disk interface. *Tribology Transactions*, 40(1):111-119. https://doi.org/10.1080/10402009708983636

Li XL, Suo SF, Guo F, et al., 2018. A study of reciprocating seals with a new mixed-lubrication model based on inverse lubrication theory. *Lubrication Science*, 30(3):126-136. https://doi.org/10.1002/ls.1410

Meng XK, Bai SX, Peng XD, 2014a. An efficient adaptive finite element method algorithm with mass conservation for analysis of liquid face seals. *Journal of Zhejiang University-SCIENCE A (Applied Physics & Engineering)*, 15(3):172-184. https://doi.org/10.1631/jzus.A1300328

Meng XK, Bai SX, Peng XD, 2014b. Lubrication film flow control by oriented dimples for liquid lubricated mechanical seals. *Tribology International*, 77:132-141. https://doi.org/10.1016/j.triboint.2014.04.020

Nikas GK, 2003. Elastohydrodynamics and mechanics of rectangular elastomeric seals for reciprocating piston rods. *Journal of Tribology*, 125(1):60-69. https://doi.org/10.1115/1.1506316

Nikas GK, 2010. Eighty years of research on hydraulic reciprocating seals: review of tribological studies and related topics since the 1930s. *Proceedings of the Institution of Mechanical Engineers, Part J: Journal of Engineering Tribology*, 224(1):1-23. https://doi.org/10.1243/13506501JET607

Öngün Y, André M, Bartel D, et al., 2008. An axisymmetric hydrodynamic interface element for finite-element computations of mixed lubrication in rubber seals. *Proceedings of the Institution of Mechanical Engineers, Part J: Journal of Engineering Tribology*, 222(3):471-481. https://doi.org/10.1243/13506501JET393

Patir N, Cheng HS, 1978. An average flow model for determining effects of three-dimensional roughness on partial hydrodynamic lubrication. *Journal of Lubrication Technology*, 100(1):12-17. https://doi.org/10.1115/1.3453103

Patir N, Cheng HS, 1979. Application of average flow model to lubrication between rough sliding surfaces. *Journal of Lubrication Technology*, 101(2):220-229. https://doi.org/10.1115/1.3453329

Payvar P, Salant RF, 1992. A computational method for cavitation in a wavy mechanical seal. *Journal of Tribology*, 114(1):199-204. https://doi.org/10.1115/1.2920861

Roelands CJA, 1966. Correlational Aspects of the Viscosity-temperature-pressure Relationship of Lubricating Oils. PhD Thesis, Technische Hogeschool Delft, Delft, the Netherlands.

Ruskell LEC, 1980. A rapidly converging theoretical solution of the elastohydrodynamic problem for rectangular rubber seals. *Journal of Mechanical Engineering Science*, 22(1):9-16. https://doi.org/10.1243/JMES_JOUR_1980_022_004_02

Safar ZS, 1991. Design of hydrodynamic wavy contacting face seals with non-Newtonian lubricants. *Tribology Series*, 18:259-263.

Salant RF, Maser N, Yang B, 2007. Numerical model of a reciprocating hydraulic rod seal. *Journal of Tribology*, 129:91-97. https://doi.org/10.1115/1.2401222

Salant RF, Yang B, Thatte A, 2010. Simulation of hydraulic seals. *Proceedings of the Institution of Mechanical Engineers, Part J: Journal of Engineering Tribology*, 224(9):865-876. https://doi.org/10.1243/13506501JET709

Sharma SC, Rajput AK, 2013. Effect of geometric imperfections of journal on the performance of micropolar lubricated 4-pocket hybrid journal bearing. *Tribology International*, 60:156-168. https://doi.org/10.1016/j.triboint.2012.10.017

Sharma SC, Yadav SK, 2014. Performance analysis of a fully textured hybrid circular thrust pad bearing system operating with non-Newtonian lubricant. *Tribology International*, 77:50-64. https://doi.org/10.1016/j.triboint.2014.04.013

Shen MX, Zheng JP, Meng XK, et al., 2015. Influence of Al_2O_3 particles on the friction and wear behaviors of nitrile rubber against 316L stainless steel. *Journal of Zhejiang University-SCIENCE A (Applied Physics & Engineering)*, 16(2):151-160. https://doi.org/10.1631/jzus.A1400217

Singh C, Nailwal TS, Sinha P, 1982. Elastohydrostatic lubrication of circular plate thrust bearing with power law lubricants. *Journal of Tribology*, 104(2):243-247. https://doi.org/10.1115/1.3253187

Sinha P, Kennedy JS, Nailwal TS, 1987. Hydrostatic pressure effects in misaligned radial face seals with non-Newtonian fluids. *Wear*, 116(3):329-342. https://doi.org/10.1016/0043-1648(87)90181-5

Streator JL, 2002. A model of mixed lubrication with capillary effects. *Tribology Series*, 40:121-128. https://doi.org/10.1016/S0167-8922(02)80013-X

Stupkiewicz S, Marciniszyn A, 2009. Elastohydrodynamic lubrication and finite configuration changes in reciprocating elastomeric seals. *Tribology International*, 42(5):615-627. https://doi.org/10.1016/j.triboint.2008.08.008

Yang B, 2010. Elastohydrodynamic Model of Reciprocating Hydraulic Rod Seals. PhD Thesis, Georgia Institute of Technology, Georgia, USA.

Yang B, Salant RF, 2010. Elastohydrodynamic lubrication simulation of O-ring and U-cup hydraulic seals. *Proceedings of the Institution of Mechanical Engineers, Part*

J: Journal of Engineering Tribology, 225(7):603-610. https://doi.org/10.1177/1350650110397236

Zhao XX, Zhang SS, Wen PF, et al., 2016. Condition monitoring of reciprocating seal based on FBG sensors. *Smart Materials and Structures*, 25(7):075045. https://doi.org/10.1088/0964-1726/25/7/075045

Zhou CJ, Pan LJ, Xu J, et al., 2017. Non-Newtonian thermal elastohydrodynamic lubrication in point contact for a crowned herringbone gear drive. *Tribology International*, 116:470-481. https://doi.org/10.1016/j.triboint.2017.08.007

Zienkiewicz OC, Taylor RL, 2000. The Finite Element Method, 5th Edition. Butterworth Heinemann, Oxford, UK, p.15-23.

中文概要

题　目： 基于幂律流体模型的非牛顿流体对斯特封密封行为影响的仿真研究

目　的： 研究润滑油的非牛顿流体行为对液压往复活塞杆的斯特封密封性能的影响，为密封设计提供理论参考。

创新点： 1. 基于幂律流体模型和 JFO 空化理论，推导出同时考虑粗糙度、流体空化和非牛顿流体效应的修正雷诺方程；2. 建立非牛顿流体的混合润滑软弹流模型，探究流体流变属性对斯特封密封行为及性能的影响。

方　法： 1. 通过理论推导，建立混合润滑条件下非牛顿流体的软弹流仿真模型；2. 对比分析不同工况条件下假塑性（n<1）、膨胀型（n>1）两种典型非牛顿流体和牛顿流体（n=1）对斯特封密封行为影响的区别，揭示假塑性和膨胀型两种非牛顿流体的密封机理。

结　论： 1. 非牛顿流体效应对液压往复斯特封密封性能具有重要影响：幂律指数越大，流体的动压效应越强，密封性能越好。2. 相比于牛顿流体，膨胀型流体润滑条件较好，密封具有低摩擦低泄漏的优点；假塑性流体润滑条件较差，密封摩擦力较大，不易实现零泄漏。

关键词： 非牛顿流体；幂律流体；斯特封；软弹流